Novel EPR-Insulated DC Cables for Future Multi-Terminal MVDC Integration

Mattewos Tefferi,[1] Zongze Li,[1] Yang Cao,[1] Hiroaki Uehara,[2] and Qin Chen[3]

[1]NSF Industrial University Collaborative Research Center on High Voltage/Temperature Materials and Structures, Electrical Insulation Research Center, Institute of Materials Science, Department of Electrical and Computer Engineering, University of Connecticut, Storrs, CT, USA; [2]Department of Electrical and Electronic Engineering, Kanto Gakuin University, Yokohama, Japan; and [3]GE Global Research Center, Niskayuna, NY, USA

Key words: medium voltage direct current (MVDC), space charge, conductivity, thermal gradient, cross-linked polyethylene (XLPE), ethylene propylene rubber (EPR)

A new twist on a legacy EPR turned it into a MVDC cable insulation with superior space charge resistance to polarity reversal, well suited for multi-terminal DC grid for renewal integration and harsh environmental and marine electrifications.

Introduction

Modern power systems are undergoing a grand transformation toward a wide-area transmission network, publicly known as "Smart Grid" and "Super Grid," for technical and economic advantages. Regional systems have been built-up toward national grids and later interconnected with neighboring countries [1,2]. High-voltage direct current (HVDC), an efficient non-synchronized solution, has been widely adopted for such long-haul bulk grid interconnections with the economic benefits of reduced power loss, no reactive power, easy connection with enhanced stability [1,2]. In addition, free from reactive power loss, HVDC cables become viable solutions for submarine power transmission, urban grid decongestions, off-shore wind power integration, and harsh environment electrification. With the introduction of the voltage source converter (VSC) based HVDC system, whereby polarity reversal is not required for bi-directional power flow control, the use of extruded XLPE DC cable has out-paced the mass-impregnated (MI) cables used traditionally with line-commutated converter (LCC) systems. Over the past few years, an increasing demand of interconnectivity between transmission and distribution grids and operation flexibility with deeper penetration of renewable energies has extended DC operations from point to point transmissions into new grid topologies such as multi-terminal DC [3,4].

The multi-terminal MVDC framework naturally facilitates the deployment of distributed power sources and the integration of renewables with largely reduced number of source and load conversion stages, often at voltage level of the transmission grid, resulting in reduced transmission and conversion losses. The MVDC platform serves as an additional layer of infrastructure in the electric grid between the transmission and distribution levels, as well as a means for supplying consumers of all types. Other initiatives being explored with MVDC technology are marine electrification for future naval ship power system, linking of oil and gas platforms and subsea O&G electrification, telecommunications and IT data centers [3–5].

Despite these opportunities, significant technical challenges persist for HVDC/MVDC technology, namely in DC cabling and accessories, DC breakers and DC diagnosis and monitoring. The major challenge for DC cabling resides in the insulation due to performance deterioration by space charge accumulation. However, MVDC is often viewed as a straight forward downsizing in voltage level from HVDC, rather than a new development. Conversely, due to potential risks of polarity reversal during the steady-state operation and fault transients in multi-terminal MVDC, further development of space charge aging prone insulation is still greatly needed for enhanced performance and reliability. In this paper, a novel EPR is described to address these challenges for highly reliable and efficient multi-terminal MVDC cabling (Figure 1).

Novel EPR-Based DC Insulation

At present, extruded DC cables are based primarily on special grades of cross-linked polyethylene (XLPE) manufactured by extra clean processes, reaching a voltage level of 320 kV in recent deployments, all for VSC topology [6]. In this study, DC characteristics of a novel EPR formulated for DC were studied along with DC XLPE. EPR has excellent performances at high temperature, low water permeability as well as resistance to water trees, and has been widely used for power distribution with unmatched underground performance [7,8]. Due to its relatively high ac loss factor, EPR has limited use at transmission class (up to 150 kV). It should be noted that, under HVDC, such ac loss is no longer a limiting factor for EPR. In addition, being a filled compound, EPR possesses a wide range of material

 0883-7554/19/©2019/IEEE

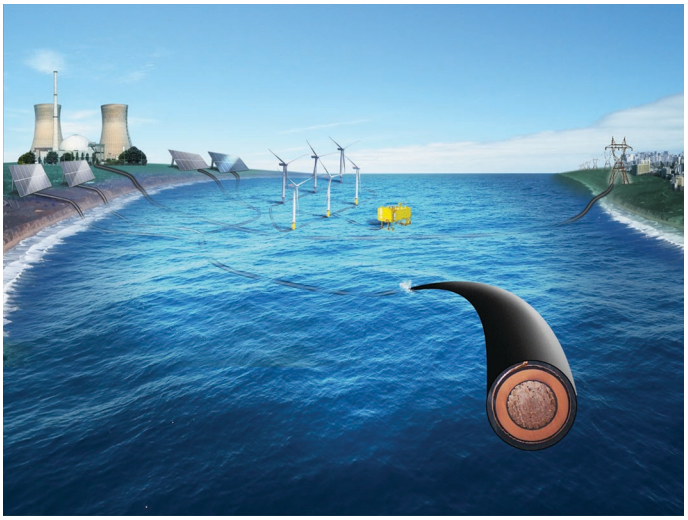

Figure 1. MVDC cabling for renewable energy integration under harsh subsea environment.

design space for engineering optimization into DC formulation. Press molded XLPE and EPR samples were prepared by using hydraulic hot press with special grades of resins provided by Electrical Cable Compounds and Kerite Company. Pressing of XLPE or EPR samples starts at 130°C allowing the melting of granulates under several tons of pressure followed by a crosslinking step at 170°C and finally cooling to room temperature. To investigate the influence of crosslinking agents on the insulation properties, two kinds of samples were studied. One was fresh sample (XLPE or EPR) readily after press molding and the other was degassed for five days at 80°C in vacuum.

Optimal Characteristics of DC Insulation

The optimal material properties of DC cable insulation include controlled DC conductivity with low temperature coefficient, low space charge accumulation, and high DC and impulse breakdown strengths. The charge injection, transport, accumulation, and recombination of space charge in extruded cable insulation, such as XLPE or EPR, deteriorate the insulating performance under HVDC. Therefore, it is essential to clarify the formation mechanism of space charge and its effect on insulation aging. In general, the temperature dependence of the electrical properties of insulating materials in HVDC power cables affects all aspects of the formation of space charges, which often develop into complicated charge patterns that evolve over time. For polymeric cable insulation, the dielectric constant is almost independent of the electric field and temperature, while the conductivity is highly sensitive to temperature [9,10]. When the load current flows through the transmission cable, a thermal gradient is generated by Joule heating in the cable conductor (Figure 2a). Furthermore, the electrical conductivity of typical polymeric insulating materials depends strongly on the temperature and hence the radial position across the transmission cable [11]. In the presence of thermal gradient, the radial spatial variation of the ratio of two electromagnetic constitutive parameters of the cable dielectric, the permittivity vs conductivity, requires, under steady-state, the presence of the space charge ρ across the insulation [12].

More specifically, the electric field distribution across the insulation material can be calculated by combining Gauss law, current continuity equation, Ohm's law and gradient of the potential, coupled with the Fourier heat conduction equation for temperature distribution across cable insulation

$$\text{Electrical Field: } \frac{\partial}{\partial t}\left[\frac{1}{r}\frac{\partial}{\partial r}\left(r\varepsilon_0\varepsilon_r\frac{\partial V}{\partial r}\right)\right]+\frac{1}{r}\frac{\partial}{\partial r}\left(r\sigma\frac{\partial V}{\partial r}\right)=0 \tag{1}$$

$$\text{Thermal Field: } \rho_m C_p\frac{\partial T}{\partial t}=\frac{1}{r}\left(rk\frac{\partial T}{\partial r}\right)+\sigma E^2 \tag{2}$$

As shown in Figures 2a and 2b, the initial Laplacian field distribution under no load condition evolves gradually to resistive field distribution under full load conditions. During this period, the field distribution will be time dependent, and the time before the DC state is reached can take from hours to days, depending on the material properties and the load condition. The nonlinear character of conductivity and strong temperature dependency lead to the complex redistribution of the electric field, often known as "electric field stress inversion" as shown in Figure 2b, which in turn manifests the space charge build-up in the cable. Shown in Figure 2c, under cylindrical coordinate, the radial spatial variation of the ratio of the permittivity vs conductivity, induces the formation of the space charge ρ across the insulation (i.e., spatial uniform dielectric time constant $\tau = \varepsilon/\sigma \neq$ constant), the time evolution of which is given by:

$$\text{Space charge: } \rho=\frac{\varepsilon}{\sigma}\frac{\partial\rho}{\partial t}+J\cdot\nabla\left(\frac{\varepsilon}{\sigma}\right) \tag{3}$$

For new DC insulation development, the ambition is to keep the temperature coefficient of the conductivity as low as possible, to avoid high local field due to the formation of space charges in the presence of the expected temperature gradient at operating temperature and electric field. The presence of space charge can lead to harmful field enhancements, be it heterocharge or homocharge. If, in addition, voltage polarity reversal is presented (under bi-directional power flow and fault transients), the accumulation of homocharge can lead to further abnormal field distribution, causing significant field enhancement at the insulation-electrode interface. The DC conductivity of plaque specimens was measured using a three-terminal sample holder designed according to ASTM 257 specifications. Specimens of 250 μm in thickness were inserted in guarded stainless-steel electrodes for quasi steady-state current measurements by using a Keithley 6514 electrometer for 5000 s. The experimentally obtained conductivity data were fitted to a simplified conductivity model to assess their dependence on electric field and temperature

$$\sigma(T,E)=\sigma_0\exp(\alpha T)\exp(\beta E). \tag{4}$$

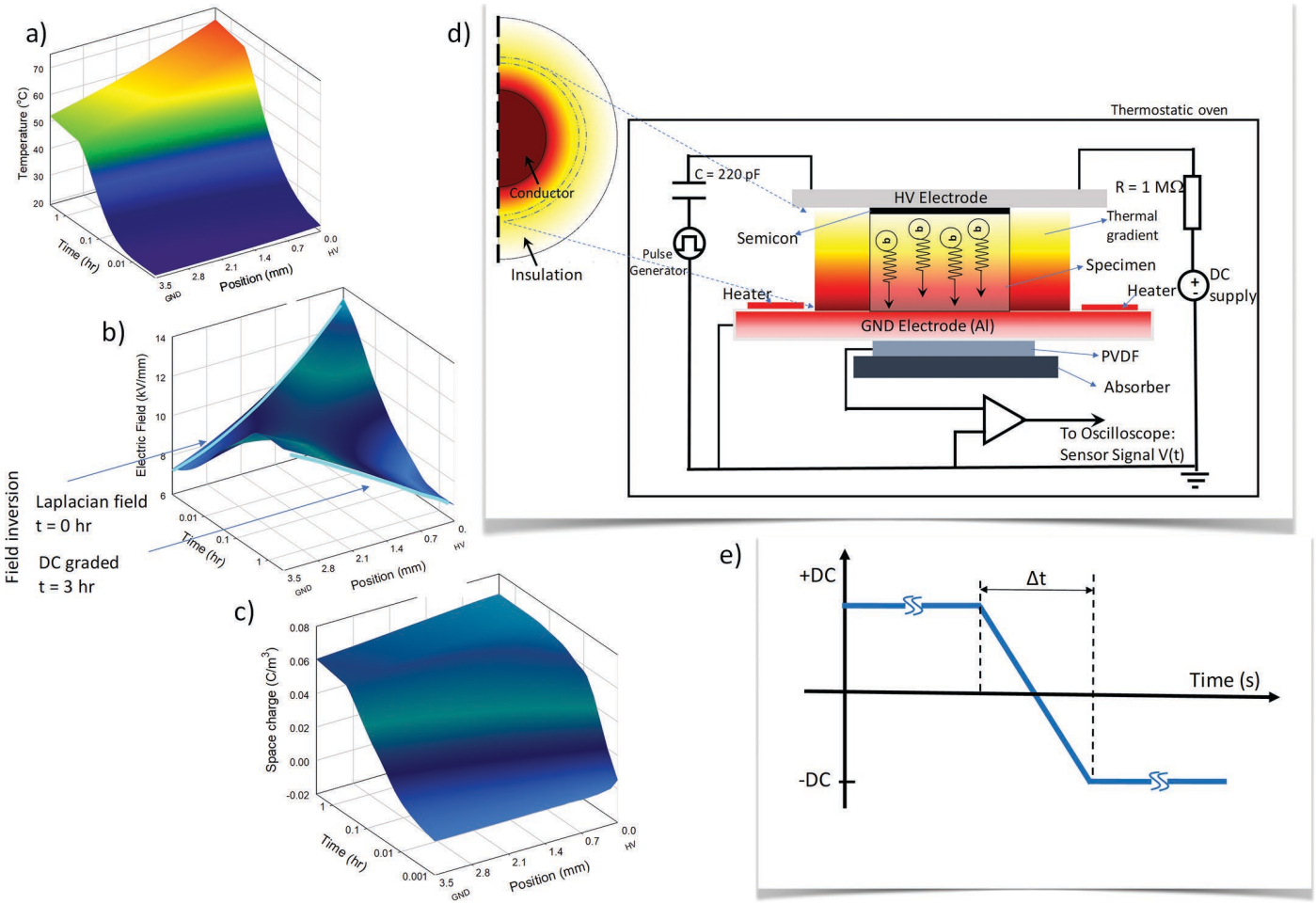

Figure 2. Temporal and spatial distribution of (a) temperature (b) electric field and (c) space charge, all based on electro-thermal coupled Multiphysics modeling of a model cable with electrical parameters listed in Table 1. (d) Modified PEA system for thermal gradient generation to account for the load condition for cables in service. Space charge measurements were performed with $\Delta T \approx 1.2$°C across slab samples of ~1mm with varying ambient temperature to "scan" radially through the cable insulation. (e) Voltage polarity reversal application procedure.

where σ_0 is the conductivity at reference temperature, E is the electric field, T is the temperature, α is the temperature coefficient, and β is the field stress coefficients of the insulation. As shown in Table 1, the temperature coefficient of the electrical conductivity for EPR is much lower compared with XLPE, indicating EPR is much better suited for DC than XLPE. Due to the complex nature of space charge formation, transport and trapping, new EPR formulation is further characterized experimentally for its space charge characteristics under simultaneous electrical and thermal gradients.

Space Charge Characterization

For power cable under typical load conditions, a temperature gradient of 5–15°C is developed with the surface temperature of the cable reaching ~50°C. Per analysis aforementioned, such thermal gradient may result in the accumulation of space charge. A modified pulsed-electroacoustic (PEA) system was developed so that the space charge behavior in thin films under thermal gradient could be investigated. Figure 2d shows schematically the enhanced PEA system with a specially designed electric heating system for thermal gradient generation across a flat sample. Thin film electric heaters were incorporated to heat up the bottom aluminum electrode to generate sufficient and laterally uniform thermal gradient across the sample. A feedback loop was provided for proportional-integral-derivative (PID) temperature control by deploying a resistor temperature detector (RTD) sensor to monitor the temperature on both the upper and lower surfaces of the specimen. The PEA sample cell is housed in a thermostatic oven for ambient temperature adjustment [13,14]. Results reported in this paper are based on a

Table 1. Conductivity parameters for XLPE and EPR

Parameter	XLPE	EPR
σ_0 (S/m)	1.4E-23	2.4E-21
α (1/K)	0.064	0.044
β (m/V)	6.7E-08	6.5E-08

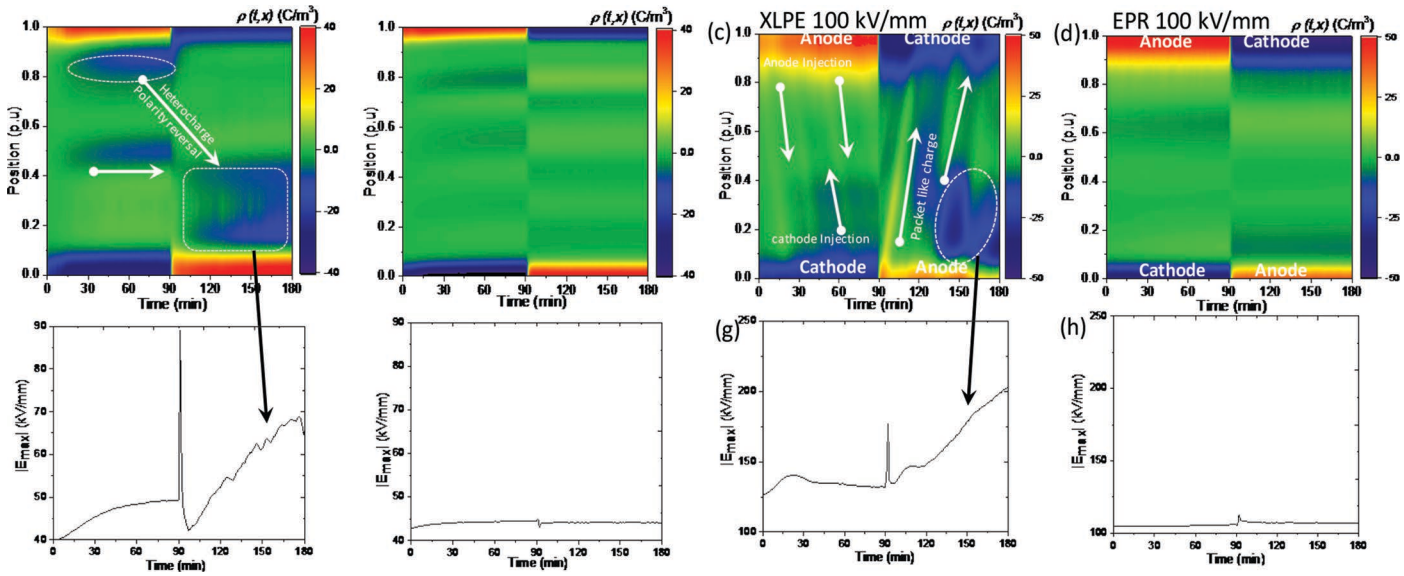

Figure 3. Space charge distribution of fresh EPR and XLPE samples under ± 40 kV/mm and ± 100 kV/mm (a-d) and corresponding temporal maximum field distribution (e-h).

thermal gradient of $\Delta T = 1.2°C/mm$, with the ambient temperature maintained at 50°C.

In this study, XLPE and EPR were hot pressed into thin films of 4 cm × 4 cm in size and ~250 μm in thickness. All specimens were metallized with 80/20 wt% gold/palladium electrodes of 1 cm diameter on both sides. To improve acoustic impedance matching between the sample and the electrodes, a small amount of silicone oil was put between them. A semiconducting (SC) layer was used between the high voltage metal electrode and the sample to minimize the mismatch of acoustic impedance, while the metallized sample was put directly on a grounding aluminum (Al) electrode [15]. Ten ns, 350 V pulse train with ~1 ns rise time and a repetition of 150 Hz was applied to slab samples under simultaneous electrical and thermal gradients. Acoustic pulses were generated in the presence of excessive charges in the sample under test and traveled through an acoustic delay line to the 10 um PVDF piezoelectric sensor, the output of which was pre-amplified for recording with a Tektronix DPO5034 oscilloscope with a sampling rate of 2.5 GS/sec. All data trace was averaged over 5000 measurements before further digital signal processing.

The nominal electric field of a typical DC polymeric cable is designed to be 10–20 kV/mm. During the prequalification test (load cycle test) of the actual DC cable, a polarity reversal test is performed by applying 1.45 times the nominal operation voltage level [16]. Thus, the polarity reversal was studied under ± 40 kV/mm. In addition, higher field of ± 100 kV/mm was applied to study the space charge dynamics under extreme conditions. Figure 2e shows a schematic diagram of voltage polarity reversal. First, the sample was stressed to a positive voltage and the time dependent space charge distribution was measured for 90 min. Then the voltage polarity was reversed by ramping the voltage level from positive to negative with a constant ramping rate over 1 min. After the polarity reversal, corresponding space charge distribution was measured for 90 min.

Figure 3 shows the space charge cartography with corresponding maximum electric field in fresh XLPE and fresh EPR under a positive half cycle followed by a negative half cycle. In Figures 3a to d, the space charge density distributions are described using color map corresponding to the color bar on the right-hand side of each plot. In Figures 3e to h, the evolution of the maximum electric filed at a given location is plotted. In the absence of space charge, the maximum electric field is nearly equal to the average applied field (Laplacian field). In case of space charge accumulation, the maximum electric field will be higher or lower than the average field depending on the type of space charge presence. In case of heterocharges accumulated close to the electrode, the electric field will be higher than the average field. On the other hand, homocharges result in field lower than the average applied field. As shown in Figure 3a, for fresh XLPE, no active space charge was observed during the first 20 min. However, after 30 min, heterocharges start to accumulate near the anode. Due to ionization of crosslinking residuals under DC stress, packet-like charges are also observed in the bulk. After polarity reversal, once again these heterocharges appear and gradually buildup close to the anode with time. Due to the presence of heterocharges before and after polarity reversal, the maximum electric field increases with time and the peak value reaches above 65 kV/mm. On the other hand, for fresh EPR during positive and negative cycles, no obvious charge accumulation was observed. Thus, the electric field appears to be homogeneous and stable in the bulk. The maximum electric field is about 42 kV/mm which is within experimental error to the applied average stress of 40 kV/mm.

Figures 3c and d, show the space charge patterns under high field. The space charge distribution for fresh XLPE shows more complex behavior. At the anode side, homocharge injection takes place immediately after the application of positive voltage. This homocharge injection dominated the first half cycle. The injected packet-like charge moved toward the cathode side.

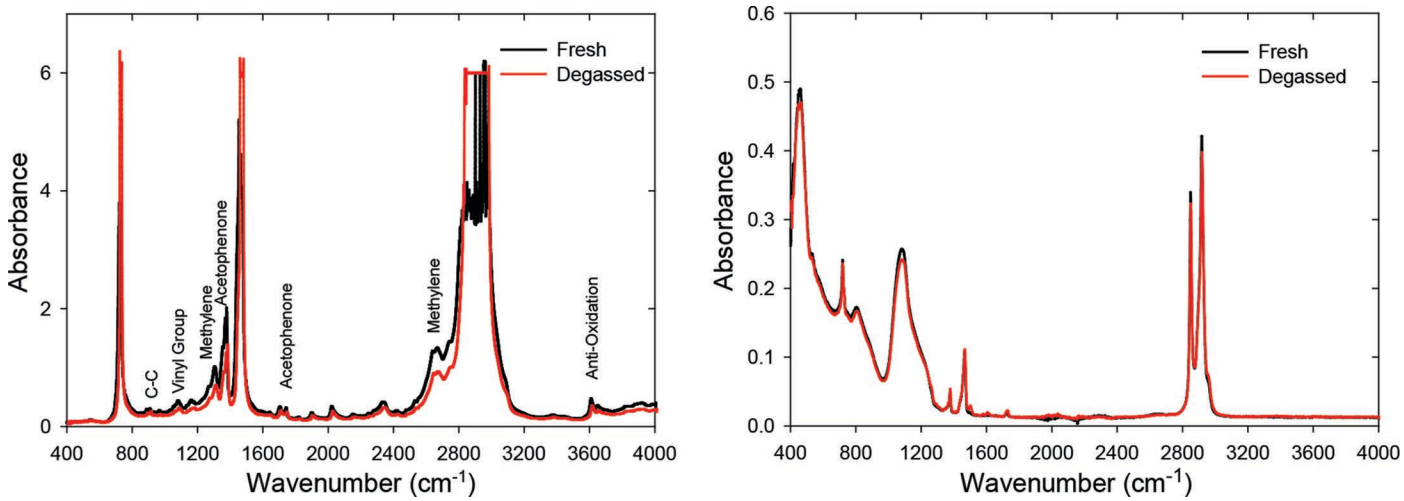

Figure 4. FTIR absorbance spectra of fresh and degassed XLPE (a) and EPR (b).

Shortly after polarity reversal, strong homocharge injection from the anode side was observed. This homocharge injection increases up to 130 min. After 130 min, homocharge injection no longer occurs and heterocharge accumulation can be observed. Consequently, the electric field was enhanced significantly and reached a peak value of about 200 kV/mm which is twice as large as the applied stress of 100 kV/mm. For the case of EPR, during positive half applied voltage, the space charge distribution remained uniform. Nevertheless, after polarity reversal a small portion of heterocharge accumulated near the anode. As a result, field is enhanced <5%.

Effect of Sample Degassing and Impact on Cable Manufacturing

The thermal and mechanical properties of polyethylene can be significantly enhanced by the crosslinking process during which the polymer structure is modified through the formation of chemical bonds between the polymer chains [17]. However, the residual crosslinking byproducts can act as impurities which significantly affect the properties of XLPE cables. Degassing is one of the material treatment processes commonly employed in cable manufacturing at moderately high temperature thereby removing volatile residual by-products to improve insulation performance [18]. The Fourier Transform Infrared (FTIR) spectra of fresh and degassed XLPE and EPR are shown in Figure 4. From the spectra of fresh and degassed XLPE (Figure 4a), it can be seen that degassing treatment can lead to a large reduction in vinyl group, acetophenone and methylene which are located at 1110 cm^{-1}, 1300 cm^{-1} and 2700 cm^{-1}, respectively. Tested in a similar way, FTIR-ATR spectra for fresh and degassed EPR samples exhibit no obvious difference (Figure 5b), which suggests good oxidative stability.

Figures 5a and b show the time dependent space charge distribution in degassed XLPE and EPR under ±40 kV/mm, respectively. For the case of degassed XLPE, at the beginning,

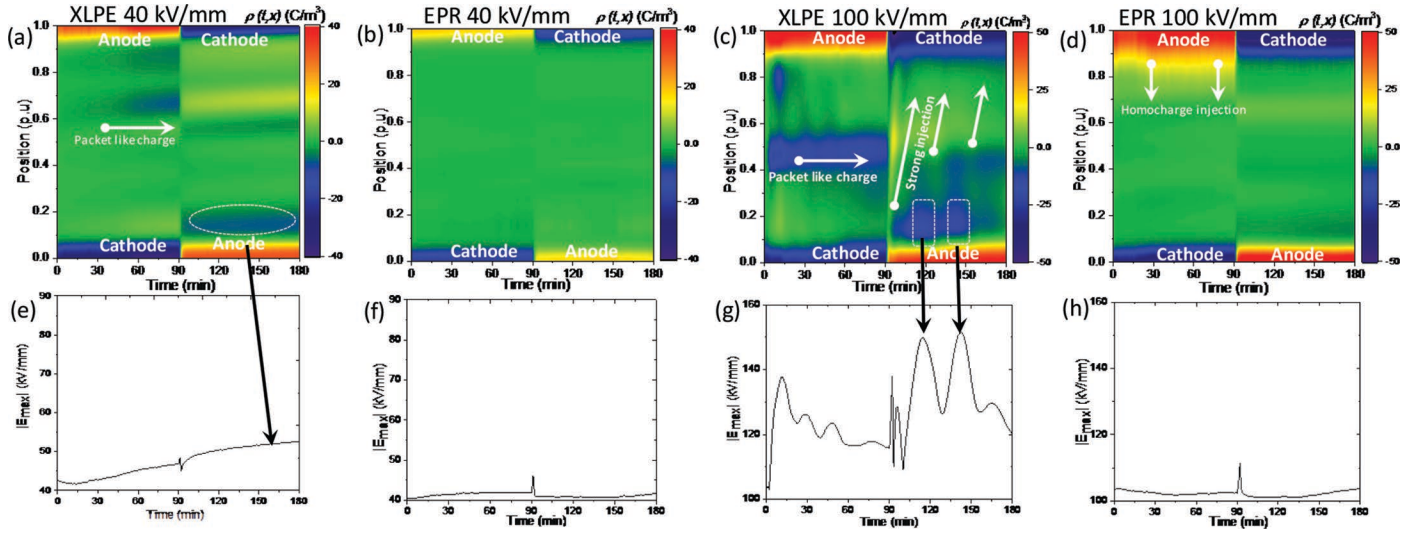

Figure 5. Space charge distribution of degassed EPR and XLPE samples under ± 40 kV/mm and ± 100 kV/mm (a-d) and corresponding temporal maximum field distribution (e-h).

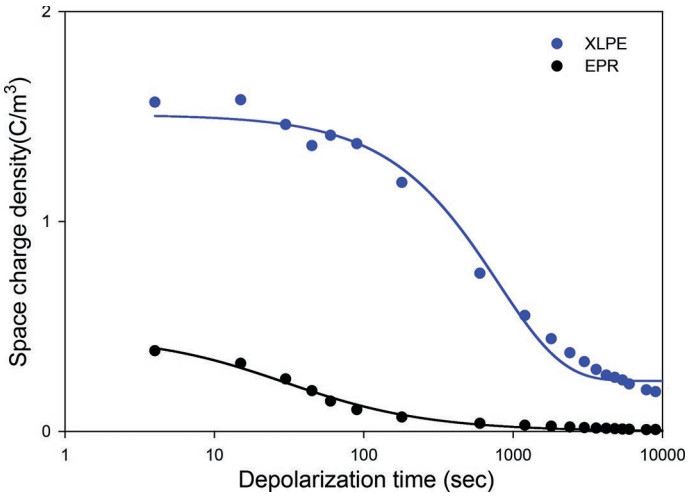

Figure 6. Depolarization characteristic determined according to equation (5). Measured value (symbol), fitted curve (solid lines). Measurements started 5 s after voltage removal, poling field = 40 kV/mm, XLPE (a) and EPR (b).

homocharges can be observed near the anode. In the vicinity of the cathode side, no charge is accumulated. Before the polarity reversal (starting at 80 min), heterocharge distribution starts to dominate near the anode. As a result, the maximum field starts to increase with time. Immediately after polarity reversal, those heterocharges dominate anode side and as a result the maximum field increases with time. Regarding EPR, no noticeable space charge accumulation was observed during positive and negative cycles. As a result, the field remained uniform. Figures 5c and d show the measurement results obtained under ±100 kV/mm for degassed XLPE and EPR. For degassed XLPE, during the positive half cycle homocharge injection near the anode and packet-like charge in the bulk were observed and the enhanced field was about 130kV/mm (about 30% increase). Immediately after polarity reversal (90–92 min), strong injection was observed from the anode side and positive space charge moved from anode to cathode. This resulted in field distortion inside the insulator and local field concentration during polarity reversal. In the case of EPR, during positive cycle relatively small homocharge injection was observed near the positive electrode. Beside this, no active space charge dynamic was observed and packet-like charges were not formed.

Comparing Figure 5 with Figure 3, a large portion of space charge in XLPE sample is reduced by degassing. The maximum electric field for degassed XLPE is much smaller than fresh XLPE. On the other hand, degassed EPR shows similar behavior to fresh EPR. Therefore, degassing treatment provides insignificant improvement for EPR.

Figure 6 shows the space charge characteristics during depolarization of XLPE and EPR during the depolarization after removal of 3 h. stressing. It can be seen for XLPE that charge decreases at a relatively slow rate whereas, the charges dissipate fairly fast in the case of EPR. The relaxation time was calculated from the measured space charge using equation 5.

$$\rho(t) = \rho_0 \exp(-t/\tau) + \rho_\infty, \qquad (5)$$

where $\rho(t)$ is the space charge density at time t, with $t = 0$ corresponding to the instant when the voltage is turned off, τ is the space charge relaxation time constant.

The space charge relaxation time constant, calculated from Figure 6 using equation (5), yields, $\tau = 800$ sec, $\tau = 50$ sec for XLPE and EPR, respectively. Since the relaxation time constant of EPR is faster than XLPE, the redistribution of space charge can follow the change of voltage and hence minimize the electric field enhancement during the voltage polarity reversal.

Degassing is one of the material treatment processes commonly employed in XLPE cable manufacturing to improve insulation performance. The improvement of insulation performance is always attributed to the removal of volatilization of crosslinking byproducts in the finished cable insulation. Longer degassing of cable is not favorable from a cable production perspective as it is capacity demanding as well as time and energy consuming.

The fact that degassing provides insignificant improvement in EPR, makes it suitable from a cable production point of view. If the time-consuming degassing stage of the cable production is eliminated, the lead-time for cable production will be as fast as possible. In addition, production cost associated with extrusion process and any quality assurance tests are reduced [19].

Conclusion

A novel EPR insulation has been developed for DC application and fully characterized in comparison with DC grade of XLPE. It is found that the new EPR formulation has much lower temperature coefficient and hence more stable DC field grading character. Further studies of space charge and maximum field enhancement in XLPE and EPR with or without degassing under polarity reversal for fields at ±40 kV/mm and ±100 kV/mm with thermal gradient under an ambient temperature of 50°C were carried out by using a modified PEA system.

From the space charge measurement results, a relatively large amount of space charge accumulation is observed in fresh XLPE sample. This is due to crosslinking byproducts that act as impurities. Degassing fresh XLPE reduces the accumulation of space charge and improves the maximum field enhancement. Conversely, degassing treatment provides insignificant improvement for EPR. This might be due to the characteristics of EPR such as lower crystallinity and filled nature, which, when properly engineered, suppress the formation and accumulation of space charge. The presence of carbon-carbon double bonds in XLPE results in less stability in the presence of thermal gradient [20]. This leads to a huge accumulation of space charge under thermal gradient.

At high field, a relatively large amount of positive packet-like charge was injected into XLPE from the anode electrode before and after the polarity reversal. The accumulation of the space charge increased the local electric field significantly. Thus, XLPE as insulating medium of DC cable for HVDC system accompanied by polarity reversal may become a problem. On the other hand, for the case of EPR, no obvious space charge was observed in the bulk during both cycles of polarity reversal, and the maximum electric field was stable with the value close

to the applied electric field. Hence, it can be considered that EPR is a suitable insulating material for DC cable.

References

[1] D. Fabiani, G. C. Montanari, C. Laurent, G. Teyssedre, P. H. F. Morshuis, R. Bodega, L. A. Dissado, A. Campus, and U. H. Nilsson, "Polymeric HVDC cable design and space charge accumulation. part 1: insulation/semicon interface," *IEEE Elec. Insul. Mag.*, vol. 23, no. 6, pp. 11–19, 2007.

[2] S. Delpino, D. Fabiani, G. C. Montanari, C. Laurent, G. Teyssedre, P. H. F. Morshuis, R. Bodega, and L. A. Dissado, "Polymeric HVDC cable design and space charge accumulation. Part 2: insulation interfaces," *IEEE Elec. Insul. Mag.*, vol. 24, no. 1, pp. 14–24, 2008.

[3] G. F. Reed, B. M. Grainger, A. R. Sparacino, and M. Zhi-Hong, "Ship to grid: Medium-voltage DC concepts in theory and practice," *IEEE Power Energy Mag.*, vol. 10, no. 6, pp. 70–79, 2012.

[4] I. A. Metwally, "The evolution of medium voltage power cables," *IEEE Potentials*, vol. 31, no. 3, pp. 20–25, 2012.

[5] B. M. Grainger, G. F. Reed, A. R. Sparacino, and P. T. Lewis, "Power electronics for grid-scale energy storage," *Proc. IEEE*, vol. 102, no. 6, pp. 1000–1013, 2014.

[6] V. Englund, J. Andersson, J. O. Boström, V. Eriksson, P. O. Hagstrand, J. Jungqvist, W. Loyens, U. H. Nilsson, and A. Smedberg, "Characteristics of candidate material systems for next generation extruded HVDC cables", CIGRE Session 45, Paris, France, 2014.

[7] G. Mazzanti and G. C. Montanari, "A comparison between XLPE and EPR as insulating materials for HV cables," *IEEE Trans. Power Deliv.*, vol. 12, no. 1, pp. 15–26, 1997.

[8] M. Tefferi, Z. Li, H. Uehara, Q. Chen, and Y. Cao, "Characterization of space charge and DC field distribution in XLPE and EPR during voltage polarity reversal with thermal gradient", Annu. Rep. Conf. Electr. Insul. Dielectr. Phenom., 2017, pp.617–620.

[9] M. Tefferi, S. A. Boggs, and Y. Cao, "The material space of DC polymeric dielectrics", IEEE Electr. Insul. Conf. (EIC), 2017, pp. 429–432.

[10] S. Boggs, D. H. Damon, J. Hjerrild, J. Holboll, and M. Henriksen, "Effect of insulation properties on the field grading of solid dielectric DC cable," *IEEE Trans. Power Deliv.*, vol. 16, no. 4, pp. 456–461, 2001.

[11] D. Fabiani, G. C. Montanari, C. Laurent, G. Teyssedre, P. H. F. Morshuis, R. Bodega, and L. A. Dissado, "HVDC Cable Design and Space Charge Accumulation. Part 3: Effect of Temperature Gradient," *IEEE Elec. Insul. Mag.*, vol. 24, no. 2, pp. 5–14, 2008.

[12] T. L. Hanley, R. P. Burford, R. J. Fleming, and K. W. Barber, "A general review of polymeric insulation for use in HVDC cables," *IEEE Elec. Insul. Mag.*, vol. 19, no. 1, pp. 13–24, 2003.

[13] H. Uehara, Z. Li, Q. Chen, G. C. Montanari, and Y. Cao, "The effect of thermal gradient on space charge pattern in XLPE", Annu. Rep. Conf. Electr. Insul. Dielectr. Phenom., 2015, pp. 138–141.

[14] H. Uehara, Z. Li, Q. Chen, G. C. Montanari, and Y. Cao, "Space charge behavior under thermal gradient in cross-linked polyethylene and ethylene-propylene rubber," *Sens. Mater.*, vol. 29, no. 8, pp. 1199–1212, 2017.

[15] Y. Li, M. Yasuda, and T. Takada, "Pulsed electroacoustic method for measurement of charge accumulation in solid dielectrics," *IEEE Trans. Dielectr. Electr. Insul.*, vol. 1, no. 2, pp. 188–198, 1994.

[16] Cigré TB 496, Recommendations for testing DC extruded cable systems for power transmission at a rated voltage up to 500 kV, Cigré WG B1- 32, April 2012.

[17] L. Andersson and T. Hjertberg, "The effect of different structure parameters on the crosslinking behaviour and network performance of LDPE," *Polym.*, vol. 47, no. 1, pp. 200–210, 2006.

[18] T. Andrews, R. N. Hampton, A. Smedberg, D. Wald, V. Waschk, and W. Weissenberg, "The role of degassing in XLPE power cable manufacture," *IEEE Elec. Insul. Mag.*, vol. 22, no. 6, pp. 5–16, 2006.

[19] R. Fleming, The Kerite Company, Seymour, CT. Private communication, 2017.

[20] R. J. Arhart, "The chemistry of ethylene propylene insulation, Part I," IEEE Electr, *Insul. Mag.*, vol. 9, no. 5, pp. 31–34, 1993.

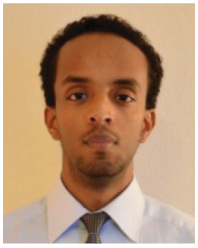

Mattewos Tefferi received his MSc in electric power engineering from Chalmers University of Technology, Sweden in 2013. He is currently pursuing his Ph.D. degree in electrical engineering at the University of Connecticut.

Zongze Li was born in Taiyuan Shanxi, China in 1991. He received the B.E. degree from Tongji University, Shanghai, China in 2014, and he is currently a Ph.D. student in the Department of Electrical and Computer Engineering in the University of Connecticut, Storrs, USA. His research is focused on high field characterization on novel materials for capacitors.

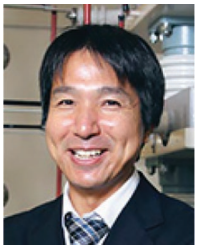

Hiroaki Uehara received his B.E., M.E., and Ph.D. degrees from Meiji University, Japan, in 1995, 1997, and 2000, respectively. In 2000, he joined the staff of the college of Engineering, Kanto Gakuin University, Japan. He was a visiting research scholar at the University of Connecticut from April 2014 to March 2015. Since 2013, he has been a professor at Kanto Gakuin University. His research interests are in insulating materials, dielectrics, and electrostatic transducers.

Qin Chen is a Senior Electrical Engineer at GE Global Research, where he has been working since 2008. His background is in dielectric materials and electrical insulation systems. His recent work focuses on the development of high voltage direct current (HVDC) components, such as subsea DC connectors, extruded HVDC cables, and HVDC converter transformers. His interest also includes the development of new polymeric and nanocomposite DC insulation materials, as well as the fundamental study of polarization and electrical charge transport in dielectric materials using both experimental and multi-physics modeling techniques. Besides HVDC

systems, his other experiences include the development of high energy density dielectric materials for energy storage film capacitors, design of AC transformers, monitoring and diagnostics of power instruments, and the study of ferroelectric polymers and developing electro-optical devices based on these materials. Qin received his BS degree from Tsinghua University (Beijing, China) in 2003, and his MS and PhD degrees from Penn State University in 2006 and 2008, all in Electrical Engineering.

Yang Cao was graduated with B.S. and M.S. in physics from Tongji University in Shanghai, China, and received his PhD from the University of Connecticut in 2002, after which he served as a senior electrical engineer at GE Global Research Center. Since 2013, he is an Associate Professor at the Electrical and Computer Engineering Department of the University of Connecticut. Dr. Cao is also the Director of the Electrical Insulation Research Center, Institute of Materials Science and the Site Director of the NSF iUCRC Center on High Voltage/Temperature Materials & Structures. His research interests are in the physics of materials under extremely high field and the development of new dielectric materials, particularly the polymeric nanostructured materials, for energy efficient power conversion and renewables integrations, as well as for novel medical diagnostic imaging devices.